Chinese Chemical Letters 33 (2022) 424–427

Contents lists available at ScienceDirect

Chinese Chemical Letters

journal homepage: www.elsevier.com/locate/cclet

Constructing low-valent Ni nanoparticles for highly selective CO_2 reduction

Kuanda Xu[1], Shisheng Zheng[1], Yang Li*, Honghao Chu, Qi Xiong, Zongwei Mei*, Qinghe Zhao, Luyi Yang, Shunning Li, Feng Pan*

School of Advanced Materials, Peking University Shenzhen Graduate School, Shenzhen 518055, China

ARTICLE INFO

Article history:
Received 6 May 2021
Revised 14 June 2021
Accepted 6 July 2021
Available online 30 July 2021

Keywords:
CO_2 reduction reaction
Ni-based catalysts
Electrocatalytic selectivity
Low-valent catalyst
DFT calculation

ABSTRACT

The electroreduction of CO_2 (CO_2RR) into value-added chemicals is a sustainable strategy for mitigating global warming and managing the global carbon balance. However, developing an efficient and selective catalyst is still the central challenge. Here, we developed a simple two-step pyrolysis method to confine low-valent Ni-based nanoparticles within nitrogen-doped carbon (Ni-NC). As a result, such Ni-based nanoparticles can effectively reduce CO_2 to CO, with a maximum CO Faradaic efficiency (FE) of 98% at an overpotential of 0.8 V, as long as good stability. Experimental and the density functional theory (DFT) calculation results reveal that low-valent Ni plays a key role in activity and selectivity enhancement. This study presents a new understanding of Ni-based CO_2RR, and provides a simple, scalable approach to the synthesis of low-valent catalysts towards efficient CO_2RR.

Electroreduction of CO_2 (CO_2RR) into chemical fuel is a promising method of carbon capture and utilization towards efficient utilization of renewable energy [1–4]. Despite the recent progress made in CO_2RR, there are currently some bottlenecks that need to be overcome en route to efficient energy conversion, including large activation barrier due to the stable chemical bond in CO_2, low selectivity limited by competing hydrogen evolution reaction (HER) and degradation of catalytic activity [5–11]. Although precious metal-based electro-catalysts, like Au [12,13], Ag [14–16], Pd [17,18] and their alloys [19–24], possess fast CO_2RR kinetics, but their low cost-efficiency impedes large-scale applications. As a result, developing the active and high-selectivity catalysts based on earth-abundant material to overcome these bottlenecks is highly desirable for CO_2RR.

Recently, transition metal nickel (Ni) has been proved to effectively convert CO_2 into CO theoretically and experimentally [25–29]. Up to now, various strategies have been proposed to design efficient Ni-based CO_2RR catalyst, including heteroatom doping engineering [30], crystal phase engineering [31,32], strain engineering [33] and nano-scale engineering [34–36]. In particular, downsizing the transition metal-based catalysts into nano-scale has been widely applied, which can increase the number of active sites and maximum metal utilization efficiency [36–38]. Besides above strategies, the valence state engineering of transition metal has been demonstrated to effectively tune the catalytic activities. To date, extensive efforts have been made in valence state engineering in different catalytic fields, such as the valence effect of MnO_x for oxygen reduction (ORR) [39], high-valence engineering for oxygen evolution (OER) [40], and Mo-valence state adjustment for optimizing hydrogen evolution (HER) [41]. Nevertheless, the study of effect of valence state on Ni-based CO_2RR catalyst is far from satisfaction. Therefore, it is highly desired to combine the downsizing the transition metal with valence state engineering for designing a more efficient CO_2RR catalyst.

Here, we developed a simple two-step high temperature reduction strategy to construct low-valent Ni nanoparticles on N-doped carbon layer as electro-catalyst (Ni-NC). Such a Ni-NC catalyst exhibits remarkable CO_2 electroreduction performance and high selectivity for CO. It can achieve high Faradaic efficiency (FE) over 90% for CO in wide potential range from −0.6 V to −1.1 V and gives a maximum FE reaches 98% at −0.8 V, which significantly exceed the most reported Ni-based catalyst (all potential are in reference to the RHE). Detailed electrochemical tests and DFT calculation demonstrate that the low-valent Ni should be responsible for the high selectivity for CO.

The Ni-NC was synthesized *via* a simple two-step pyrolysis method (Fig. 1a). Simply, glucose (GC), dicyandiamide (DCDA) and $NiCl_2$ was used as carbon, nitrogen and nickel source, respectively, which were mixed and sintered at 550 °C and followed by car-

* Corresponding authors.
E-mail addresses: ly2020@pku.edu.cn (Y. Li), meizw@pkusz.edu.cn (Z. Mei), panfeng@pkusz.edu.cn (F. Pan).
[1] These authors contributed equally to this work.

https://doi.org/10.1016/j.cclet.2021.07.016
1001-8417/

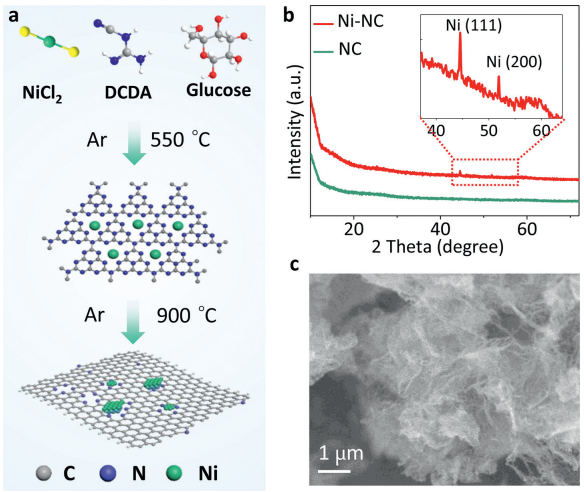

Fig. 1. Structural characterizations. (a) Schematic illustration of the synthetic procedure of Ni-NC (Ni atoms, green; N atoms, blue; C atoms, gray); (b) X-ray diffraction patterns for Ni-NC and NC; (c) SEM image of Ni-NC.

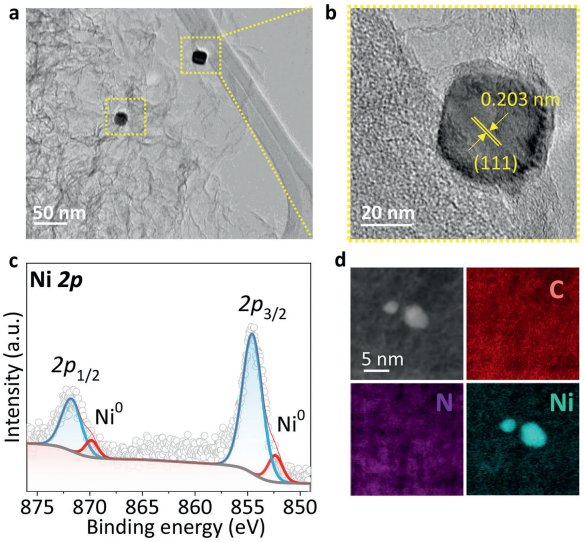

Fig. 2. (a, b) TEM image of Ni-NC; (c) Ni 2p spectrum of Ni-NC; (d) EDS mapping of Ni-NC.

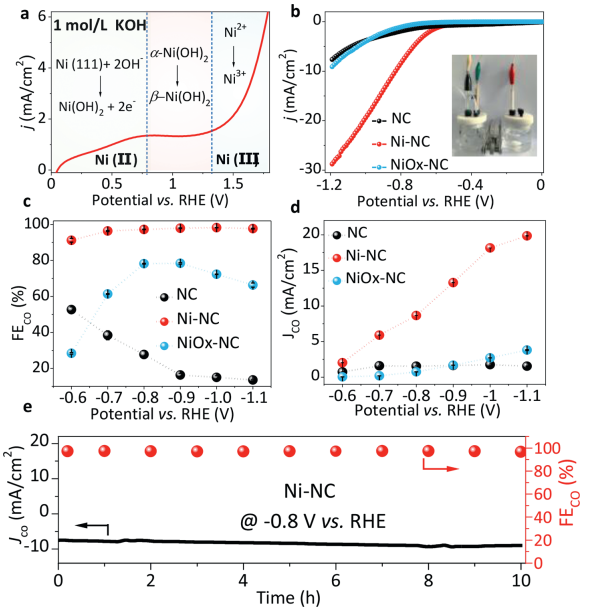

Fig. 3. Electrocatalytic CO_2RR performance. (a) LSV curves of Ni-NC in 1 mol/L KOH electrolyte at a scan rate of 10 mV/s; (b) LSV curves of Ni-NC, NiO_x-NC and NC in 0.1 mol/L $KHCO_3$; (c) Faradaic efficiency; (d) Specific current density of CO for Ni-NC, NiO_x-NC and NC at different applied potential; (e) Stability test of Ni-NC at a potential of −0.8 V *vs.* RHE for 10 h.

bonized at 900 °C under flowing Ar. The crystal structure was confirmed by X-ray diffraction (XRD) pattern in Fig. 1b. Two diffraction peaks corresponding to the (110) and (200) planes of metallic Ni are observed at 44.5° and 51.9° for Ni-NC (JCPDS, No. 71–4655) [42], which are not found in the NC counterpart. The Ni content was measured to be 7.2 wt% based on the inductively coupled plasma masss pectrometry (ICP-MS). The scanning electron microscopy (SEM) images of Ni-NC and NC exhibit a clear layered-structure morphology with folds and wrinkles (Fig. 1c and Fig. S1 in Supporting information).

To further reveal the nanostructure features of Ni-NC, high-resolution transmission electron microscopy (TEM) was performed. As shown in Fig. 2a and Figs. S2 and S3 (Supporting information), they display the carbon layer wrapped Ni nanoparticles. The lattice fringes of d = 0.203 nm in the catalysts of Ni-NC, which correspond to the (111) plane of the Ni (Fig. 2b), which is well in line with XRD data [43]. The TEM-energy dispersive X-ray spectra (TEM-EDS) mapping results show the existence of Ni, N and C elements over the nanosheets (Fig. 1d). The chemical states of Ni-NC were further investigated by X-ray photoelectron spectroscopy (XPS) (Fig. 2c and Figs. S4 and S5 in Supporting information). As shown in Fig. S5, four types of N species were distinguished, including pyridinic N (398.86 eV), pyrrolic N (399.7 eV), graphitic N (401.15 eV) and oxidized N (402.52 eV) species [44,45]. Fig. 2c displays the high-resolution of Ni spectrum of Ni-NC, Ni $2p_{3/2}$ deconvoluted in two peaks. The minor peak at 852.4 eV, which is corresponding to Ni0. The major peak at 854.6 eV is lower than Ni^{2+} (856.0 eV), suggesting the low-valent state of Ni in Ni-NC [46,47].

The electro-catalytic activities of NC, Ni-NC were studied using a H-type electrochemical cells under CO_2 saturated 0.1 mol/L $KHCO_3$. Additionally, NiO_x-NC was synthesized from Ni-NC by applying positive potential in 1 mol/L KOH, with purpose of verifying the catalytic effectiveness of low-valent Ni. As presented in Fig. 3a, the metallic Ni in Ni-NC was first oxidized to form α-$Ni(OH)_2$ and followed by oxidized to Ni^{3+} [48]. And the α-$Ni(OH)_2$ irreversibly transferred to β-$Ni(OH)_2$ during the range from 0.6 V to 1.3 V, which cannot be reduced to metallic Ni. Linear Sweep Voltammetry (LSV) displayed in Fig. 3b shows total current density at the voltage range from 0 to −1.2 V *vs.* RHE. The total current density of both NC and NiO_x-NC at −1.2 V were close to 10 mA/cm^2, while the total current density of Ni-NC almost reached 30 mA/cm^2, suggesting prominent electrocatalytic activity of Ni-NC due to the existence of low-valent Ni in Ni-NC. Faradaic efficiency (FE) and partial current density of CO were displayed respectively in Figs. 3c and d. Compared with the FE of CO exceeding 92% at the voltage range from −0.6 V to −1.1 V catalyzed by Ni-NC, the maximum FE of CO over NiO_x-NC is just close to 80%. Furthermore, the maximum FE of CO over NC is as low as 53%, even falling to no more than 10% at more negative potential. Consequently, CO partial current density of Ni-NC is much higher than the other counterparts at the whole voltage range applied. This loss in performance of NiO_x-NC is likely the result of Ni oxidation [27], which diminished the active site from metallic Ni after applying positive potential. The stability of the Ni-NC catalyst was tested by continuous working at −0.8 V for more than 10 h, both the current density and Faradaic efficiency stayed stable as presented in Fig. 3e. This result evidenced the metallic Ni would provide the active sites. And XRD pattern, TEM images together with high-resolution XPS Ni 2p

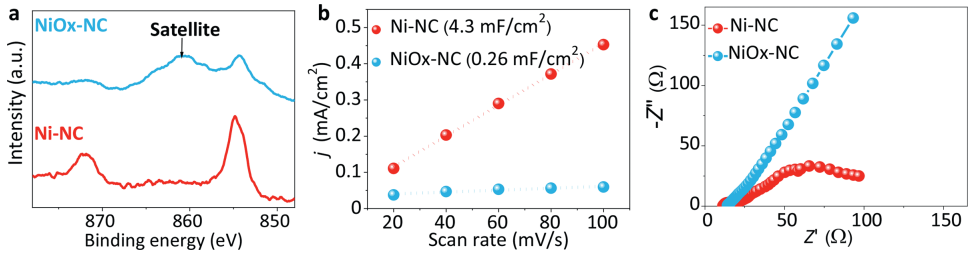

Fig. 4. (a) The XPS spectra of Ni in the Ni-NxC and NiO_x-NC (the intensity has been normalized for the comparison); (b) A plot of changing current density against scan rates for electrochemically active surface area (ECSA); (c) Electrochemical impedance spectra of Ni-NC and NiO_x-NC.

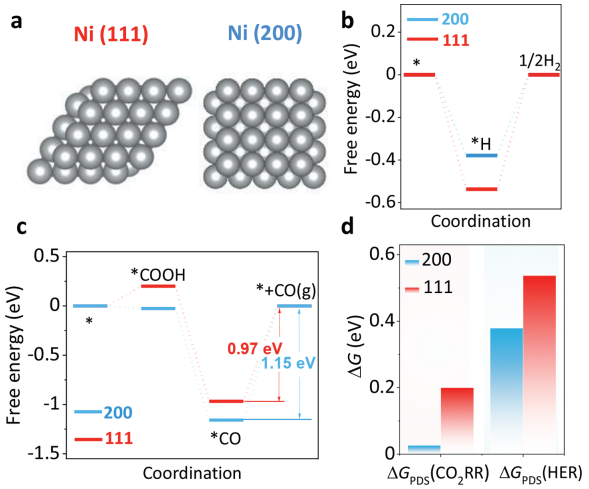

Fig. 5. DFT calculation. (a) Calculated atomic structure model of Ni (111) and Ni (200); (b) The calculated free energy diagram of HER on Ni (111) and Ni (200); (c) Calculated free energy diagram of reducing CO_2 to CO over Ni (111) and Ni (200); (d) The comparison between the free energy of potential-determining step (PDS) of CO_2RR and HER.

spectra suggest that the excellent structural and chemical stability of the Ni-NC during the CO_2RR process (Figs. S6 and S7 in Supporting information).

The oxidation of Ni during the positive potential scanning studied by XPS. The result in Fig. 4a demonstrate that the binding energy for Ni in NiO_x-NC has an obvious shakeup satellite signal at 861.1 eV, which is attributed to the Ni^{2+} [49]. This observation illustrates the surface oxidation of Ni element. The electrochemical active surface area (ECSA) of catalyst was determined to study the factor of CO_2RR activity enhancement. The ECSA of Ni-NC and NiO_x-NC were evaluated by double-layer capacitance (C_{dl}) depend on CV curves (Figs. S7a and b in Supporting information). The C_{dl} can be obtained by determining the slope of the fitted plots. The C_{dl} of Ni-NC is 4.3 mF/cm^2, which is nearly 16.5 times as high as NiO_x-NC (0.26 mF/cm^2) (Fig. 4b), indicating that the oxidation process dramatically decreases the active sites. Furthermore, electrochemical impedance spectrum (EIS) was performed to evaluate the reaction kinetics. The Ni-NC exhibits smaller charge transfer resistances than that of NiO_x-NC (Fig. 4c), suggesting its fast charge transfer kinetics. These results further demonstrate the excellent electrochemical properties of Ni-NC due to the existence of low-valent Ni.

DFT calculations were performed to reveal the mechanism of the extremely high-selectivity electrocatalytic CO_2RR process on Ni-NC. According to the observed experimental results, models of (111) and (200) feces in metallic Ni were built and presented in Fig. 5a, subsequently the free energy diagram of CO_2RR process were calculated and presented in Fig. 5c. The free energy change for *COOH formation ($CO_2 + (H^+ + e^-) \rightarrow$ *COOH + H_2O) in Ni (111) is 0.2 eV, while in Ni (200) is −0.03 eV. After the *COOH formation, *CO formation from *COOH (*COOH + $(H^+ + e^-) \rightarrow$ *CO + H_2O) is exothermic on both faces. It can be seen that, the H^+/e^- steps in both faces can proceed with low free energy, which indicates that the *CO species may easily form in both faces under potential condition of experiment. And the free energy change for CO desorption (*CO → CO(g) + *), which cannot be tune by the external potential, is more endothermic Ni (200) than that in Ni (111), this indicates that the Ni (200) would be more easily poisoned by *CO and the desorption of *CO in Ni (111) is more easily. We also examined the selectivity between the CO_2RR process and HER process (Figs. 5b and d). We compared the free energy change of potential-determining step (PDS) of CO_2RR and HER on both faces, the ΔG_{PDS} (CO_2RR) is smaller than the ΔG_{PDS} (HER), suggesting that the CO_2 reduction process is thermodynamically more favorable than that of HER, identical with the experimental high-selectivity of CO.

In summary, low-valent Ni-based nanoparticles were successfully constructed on carbon layer (Ni-NC) *via* a two-step pyrolysis method. Notably, the Ni-NC exhibited high-selectivity for CO. The Faradaic efficiency of CO was as high as 98% at overpotential of −0.8 V *vs.* RHE, with good stability over 10 h. In contrast, a significant decrease in CO_2 reduction activity was observed after low-valence Ni was oxidized, resulting from the decreasing active sites. Experimental and theoretical studies indicate that Ni (111) on Ni-NC may be a type of active site for CO_2RR, originating from more favorable initiation of CO_2 reduction than HER. This discovery not only pays a new path for design of high-selectivity to CO_2 reduction, but also presents new understanding of Ni-based CO_2 reduction.

Declaration of competing interest

The authors declare that they have no known competing financial interests or personal relationships that could have appeared to influence the work reported in this paper.

Acknowledgments

The authors also would like to acknowledge the financial support from the Shenzhen Science and Technology Research Grant (No. JCYJ20200109140416788, China), the Chemistry and Chemical Engineering Guangdong Laboratory (No. 1922018, China) and National Key R&D Program of China (No. 2020YFB0704500).

Supplementary materials

Supplementary material associated with this article can be found, in the online version, at doi:10.1016/j.cclet.2021.07.016.

References

[1] O.S. Bushuyev, P. De Luna, C.T. Dinh, et al., Joule 2 (2018) 825–832.
[2] S. Nitopi, E. Bertheussen, S.B. Scott, et al., Chem. Rev. 119 (2019) 7610–7672.

[3] Y. Zheng, A. Vasileff, X. Zhou, et al., J. Am. Chem. Soc. 141 (2019) 7646–7659.
[4] T. Wang, J. Yang, J. Chen, et al., Chin. Chem. Lett. 31 (2020) 1438–1442.
[5] P. De Luna, C. Hahn, D. Higgins, et al., Science 364 (2019) 350.
[6] S. Gao, Y. Lin, X.C. Jiao, et al., Nature 529 (2016) 68–71.
[7] T.T. Zheng, K. Jiang, H.T. Wang, Adv. Mater. 30 (2018) 1802066.
[8] Z.W. Seh, J. Kibsgaard, C.F. Dickens, et al., Science 355 (2017) 6321.
[9] M.B. Ross, P. De Luna, Y.F. Li, et al., Nat. Catal. 2 (2019) 648–658.
[10] D.D. Zhu, J.L. Liu, S.Z. Qiao, Adv. Mater. 28 (2016) 3423–3452.
[11] G. Li, Y. Qin, Y. Wu, et al., Chin. J. Catal. 41 (2020) 830–838.
[12] W. Zhu, R. Michalsky, O.n. Metin, et al., J. Am. Chem. Soc. 135 (2013) 16833–16836.
[13] S. Yu, A.J. Wilson, J. Heo, et al., Nano Lett. 18 (2018) 2189–2194.
[14] J. Rosen, G.S. Hutchings, Q. Lu, et al., ACS Catal. 5 (2015) 4293–4299.
[15] M.R. Singh, Y. Kwon, Y. Lum, et al., J. Am. Chem. Soc. 138 (2016) 13006–13012.
[16] F.P.G. De Arquer, C.T. Dinh, A. Ozden, et al., Science 367 (2020) 661–666.
[17] B. Jiang, X.G. Zhang, K. Jiang, et al., J. Am. Chem. Soc. 140 (2018) 2880–2889.
[18] H. Huang, H. Jia, Z. Liu, et al., Angew. Chem. Int. Ed. 129 (2017) 3648–3652.
[19] D. Kim, C.L. Xie, N. Becknell, et al., J. Am. Chem. Soc. 139 (2017) 8329–8336.
[20] M. Liu, Y.J. Pang, B. Zhang, et al., Nature 537 (2016) 382–386.
[21] D. Kim, J. Resasco, Y. Yu, et al., Nat. Commun. 5 (2014) 1–8.
[22] W.L. Zhu, R. Michalsky, O. Metin, et al., J. Am. Chem. Soc. 135 (2013) 16833–16836.
[23] C.T. Dinh, F.P.G. de Arquer, D. Sinton, et al., ACS Energy Lett. 3 (2018) 2835–2840.
[24] W. Luc, C. Collins, S. Wang, et al., J. Am. Chem. Soc. 139 (2017) 1885–1893.
[25] X. Li, W. Bi, M. Chen, et al., J. Am. Chem. Soc. 139 (2017) 14889–14892.
[26] Y. He, Y. Li, J. Zhang, et al., Nano Energy 77 (2020) 105010.
[27] C. Zhao, Y. Wang, Z. Li, et al., Joule 3 (2019) 584–594.
[28] S. Liu, H.B. Yang, S.F. Hung, et al., Angew. Chem. Int. Ed. 59 (2020) 798–803.
[29] Q. He, B. Wu, Y. Hu, et al., Sci. China Chem. 63 (2020) 1716–1720.
[30] Z. Ou, C. Qin, J. Niu, et al., Int. J. Hydrog. Energy 44 (2019) 819–834.
[31] K. Czelej, K. Cwieka, K.J. Kurzydlowski, Catal. Commun. 80 (2016) 33–38.
[32] W. Yang, H.J. Wang, R.R. Liu, et al., Angew. Chem. Int. Ed. 60 (2021) 409–414.
[33] R.P. Jansonius, L.M. Reid, C.N. Virca, et al., ACS Energy Lett. 4 (2019) 980–986.
[34] H. Liu, Y. Zhu, J. Ma, et al., Adv. Funct. Mater. 30 (2020) 1910534.
[35] Z. Li, D. He, X. Yan, et al., Angew. Chem. Int. Ed. 132 (2020) 18731–18736.
[36] R. Sun, Y. Liao, S.T. Bai, et al., Energy Environ. Sci. 14 (2021) 1247–1285.
[37] L. Liu, A. Corma, Chem. Rev. 118 (2018) 4981–5079.
[38] S. Zhao, R. Jin, R. Jin, ACS Energy Lett. 3 (2018) 452–462.
[39] Q. Tang, L. Jiang, J. Liu, et al., ACS Catal. 4 (2014) 457–463.
[40] B. Zhang, L. Wang, Z. Cao, et al., Nat. Catal. 3 (2020) 1–8.
[41] S. Kim, C. Choi, J. Hwang, et al., ACS Nano 14 (2020) 4988–4999.
[42] B. Zhao, Z. Chen, X. Yan, et al., Top Catal. 60 (2017) 879–889.
[43] J. Li, P. Li, J. Li, et al., Catalysts 9 (2019) 506.
[44] H. Huang, R. Xu, Y. Feng, et al., Adv. Mater. 32 (2020) 1904320.
[45] H. Wang, F. Lu, C. Ma, et al., J. Mater. Chem. B 9 (2021) 125–130.
[46] Y. Chen, J. Kang, B. Chen, et al., J. Phys. D: Appl. Phys. 45 (2012) 065303.
[47] B. Liu, T. Zhang, X. Han, et al., Angew. Chem. Int. Ed. 59 (2020) 12055–12061.
[48] S. Medway, C. Lucas, A. Kowal, et al., J. Electroanal. Chem. 587 (2006) 172–181.
[49] X. Liang, B. Liu, J. Zhang, et al., Chem. Commun. 52 (2016) 11143–11146.